Engineering Sensor Arrays Using Aggregation-Induced Emission Luminogens for Pathogen Identification

Chengcheng Zhou, Wenhan Xu, Pengbo Zhang, Meijuan Jiang, Yuncong Chen, Ryan T. K. Kwok, Michelle M. S. Lee, Guogang Shan, Ruilian Qi, Xin Zhou, Jacky W. Y. Lam, Shu Wang, and Ben Zhong Tang**

Lacking rapid and reliable pathogen diagnostic platforms, inadequate or delayed antimicrobial therapy could be made, which greatly threatens human life and accelerates the emergence of antibiotic-resistant pathogens. In this contribution, a series of simple and reliable sensor arrays based on tetraphenylethylene (TPE) derivatives are successfully developed for detection and discrimination of pathogens. Each sensor array consists of three TPE-based aggregation-induced emission luminogens (AIEgens) that bear cationic ammonium group and different hydrophobic substitutions, providing tunable log*P* (*n*-octanol/water partition coefficient) values to enable the different multivalent interactions with pathogens. On the basis of the distinctive fluorescence response produced by the diverse interaction of AIEgens with pathogens, these sensor arrays can identify different kinds of pathogens, even normal and drug-resistant bacteria, with nearly 100% accuracy. Furthermore, blends of pathogens can also be identified accurately. The sensor arrays exhibit rapid response (about 0.5 h), high-throughput, and easy-to-operate without washing steps.

1. Introduction

Microorganism identification is very important because numerous species are greatly associated with human diseases and death.[1] Currently, more than 300 million severe infection cases and over 5 million death stem from pathogens every year in the world.[2] To ensure effective treatments, rapid and reliable diagnosis of pathogen infection is the first critical step.[1b] Up to date, the most widely adopted methods for identifying microorganisms include plating and culturing, observing the morphological structure, and examining gene and immunological characteristics.[3] However, the application scopes of these techniques are limited by their inherent problems. For example, the plating and culturing method is time-consuming and usually takes several days.[4] Analyzing the morphology by microscopy hardly discriminate the pathogens with similar size and shape.[5] Examining gene and immunological characteristics of pathogens requires technologically advanced systems such as polymerase chain reaction (PCR), gene microarray, and target-specific immunoassays,[3a] which are complex and require sophisticated instrumentations. Moreover, due to multiple operating steps, the occurrence of false-positive results is unavoidable.[6] Furthermore, for some advanced technologies applied in hospitals and other authorized organizations, such as automated biochemical instrumentation and matrix-assisted laser desorption ionization time-of-flight mass spectrometry (MALDI-TOF-MS), the accuracy rate of microorganism identification is only 90–95% and several hours of operation are needed.[7] Without access to timely and reliable pathogen information, point-of-care treatment decisions were made by the prescription of a suboptimal antibiotic.[8] Under selective pressure of the suboptimal

Dr. C. Zhou, Dr. M. Jiang, Dr. Y. Chen, Dr. R. T. K. Kwok, Dr. G. Shan, Dr. J. W. Y. Lam, Prof. B. Z. Tang
HKUST Shenzhen Research Institute
No. 9 Yuexing 1st RD, South Area, Hi-tech Park, Nanshan, Shenzhen 518057, China
E-mail: tangbenz@ust.hk

Dr. C. Zhou, W. Xu, Dr. M. Jiang, Dr. Y. Chen, Dr. R. T. K. Kwok, M. M. S. Lee, Dr. G. Shan, Dr. J. W. Y. Lam, Prof. B. Z. Tang
Department of Chemistry
Hong Kong Branch of Chinese National Engineering Research Center for Tissue Restoration and Reconstruction
Department of Chemical and Biological Engineering
The Hong Kong University of Science and Technology
Clear Water Bay, Kowloon, Hong Kong 999077, China

Dr. P. Zhang, Dr. R. Qi, X. Zhou, Prof. S. Wang
Key Laboratory of Organic Solids
Beijing National Laboratory for Molecular Sciences (BNLMS)
Institute of Chemistry
Chinese Academy of Sciences
Beijing 100190, P. R. China
E-mail: wangshu@iccas.ac.cn

Prof. B. Z. Tang
State Key Laboratory of Luminescent Materials and Devices
Center for Aggregation-Induced Emission
(Guangzhou International Campus)
South China University of Technology
Guangzhou 510640, China

The ORCID identification number(s) for the author(s) of this article can be found under https://doi.org/10.1002/adfm.201805986.

DOI: 10.1002/adfm.201805986

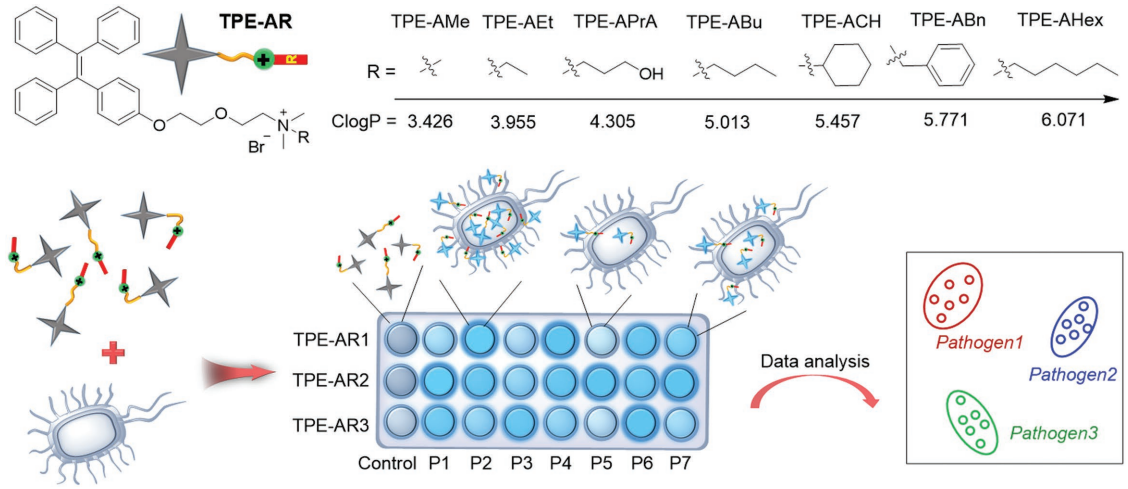

Scheme 1. Structure of TPE-ARs and schematic illustration of a sensor array composed of three TPE-ARs to achieve pathogen identification. **P1–P7** represent seven kinds of pathogens.

prescription, in which large quantities of antimicrobial agents are present or inadequate doses of drugs are taken, many strains undergo mutations and consequently acquire antibiotic resistance.[9] It has been predicted that, antibiotic-resistant infections could kill up to 10 million people worldwide by 2050.[10] Thus, a fast and reliable method to discern various pathogens is urgently required.

As an alternative, fluorescent probe is a promising tool for identifying pathogens, owing to its rich advantages, such as fast response, superior sensitivity, simplicity, and so on.[11] Some biochemical sensors based on fluorescent responses have been developed for pathogens identification.[3b,5,12] However, conventional fluorescent molecules generally suffer from the notorious aggregation-caused quenching (ACQ) effect, where their emissions are often weakened or quenched at higher concentration or in aggregated state.[13] This has confined their working concentration to a very low level, and thus limits the labeling degrees of probes to analytes, resulting in compromised sensitivity.[14] Moreover, the ACQ effect of conventional fluorophores often forces them to work in a fluorescence "turn-off" mode. Inevitably, light emissions of fluorophores are usually susceptible to some external factors such as water and air, further compromising sensitivity and accuracy of identification.[14] To overcome these issues, tailor-made quenchers were introduced to weaken the emission of fluorophore, and then the system with weak emission was used to detect bioanalysts in turn-on fashion.[12b,e,15] Although effective, this approach complicates the sensor designs.

Diametrically opposed to the conventional ACQ fluorophores, aggregation-induced emission luminogens (AIEgens) are nonemissive or weakly emissive when molecularly dissolved but highly emissive when aggregated.[16] This feature endows AIEgens with ability to work in a light-up/turn-on fashion.[17] Moreover, AIE-based probes have low background and thus without need of repeated washing procedures.[7c] These merits of AIEgens well meet the requirement of an ideal fluorescence sensor,[12e,18] which will greatly enhance the sensitivity and reliability of detection.[19] Very recently, based on the different surface electric potentials of bacteria, the sensor arrays for bacteria detection have been built using a series of AIEgens with various electric charges.[7c,20] However, the AIEgen-based sensor array showed only about 93.75% detection accuracy for bacteria samples by analyzing the collective fluorescence signals of bacteria with the statistical methods.[7c] Therefore, it still remains a great challenge to rationally design the AIEgen sensor array for enlarging the difference between fluorescence response of various pathogens and thus achieve high detection accuracy. Meanwhile, it is also significant to make the sensor arrays simple as well as improving the detection accuracy.[21]

In this work, we introduced multivalent interactions between AIEgens and pathogens to augment the diversity of the fluorescence response of pathogens, taking advantage of hydrophobic groups that are prevalent on microbial exteriors in addition to the negatively charged residues. For this purpose, a series of AIE-active tetraphenylethylene (TPE) derivatives, TPE-ARs, were designed and synthesized (**Scheme 1**). Structurally, they bear one positively charged ammonium group and different hydrophobic groups with finely controlled hydrophobicity of calculated log*P* (*Clog*P) values from 3.426 to 6.071 (log*P* is *n*-octanol/water partition coefficient, whose values were estimated using ChemBioDraw 14.0), which were engineered to tune the electrostatic and hydrophobic interactions between AIEgens and pathogens. Additionally, the alkoxy chain was introduced to increase the water-solubility and flexibility of TPE-ARs. Using these AIEgens, we successfully created multiple competent sensor arrays for rapid and reliable detection and discrimination of different pathogens, even between normal and drug-resistant pathogens, with the aid of linear discriminant analysis (LDA).

2. Results and Discussion

2.1. Synthesis and Characterization of TPE-ARs

Seven TPE-ARs (TPE-AMe, TPE-AEt, TPE-APrA, TPE-ABu, TPE-ACH, TPE-ABn, and TPE-AHex) were prepared by facile

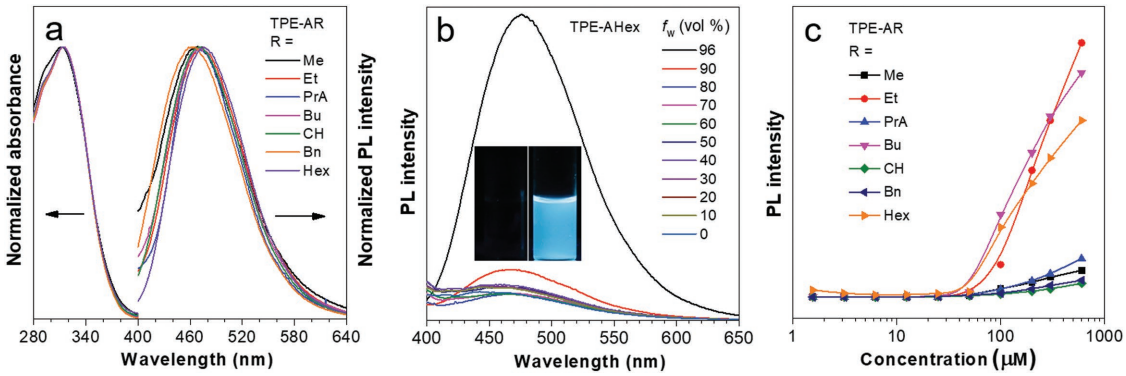

Figure 1. a) Normalized absorption spectra of TPE-ARs (20×10^{-6} M) in DMSO solution and normalized PL spectra of TPE-ARs (200×10^{-6} M) in organic solvent/H_2O mixture with 96% water fraction, λ_{ex}: 340 nm. Organic solvent/H_2O mixture: MeOH/H_2O mixture for TPE-AMe, TPE-APrA and TPE-ABn, ACN/H_2O mixture for TPE-AEt, TPE-ABu, and TPE-ACH, and DMSO/H_2O mixture for TPE-AHex. b) PL spectra of TPE-AHex (200×10^{-6} M) in DMSO/H_2O mixture with different water fraction (f_w), λ_{ex}: 340 nm. c) Plots of PL intensity of TPE-ARs versus the dye concentration in PBS solution.

synthetic routes in reasonable yields (Scheme S1, Supporting Information), and their chemical structures were fully characterized by ^{1}H NMR, ^{13}C NMR, and high-resolution mass spectra (HRMS) (Figures S1–S7, Supporting Information). Their photophysical properties were studied and summarized in Table S1 (Supporting Information). As shown in **Figure 1**a, one main absorption peak was observed at 313 or 314 nm for these AIEgens in dimethyl sulfoxide (DMSO) solution. Then, their AIE properties were studied by changing the water content in the mixtures of water-miscible organic solvent and water. Taking TPE-AHex as an example (Figure 1b), TPE-AHex emits weakly in DMSO/H_2O mixtures with water fractions from 0 to 90 vol%. Further increasing the water content to 96%, a strong emission peak at 476 nm was observed, and the difference can be easily distinguished by naked eyes (inset in Figure 1b). Similarly, at higher water fractions, the other six TPE-ARs also showed obviously enhanced fluorescence emission (Figures S8 and S9, Supporting Information), exhibiting a typical AIE phenomenon due to the formation of aggregates, as confirmed by dynamic light scattering (DLS) results (Figure S10, Supporting Information). The maximum emissions of TPE-ARs aggregates all locate at around 470 nm (Figure 1a). Thus, functionally decorating TPE in our strategy had little effect on the absorption and emission profiles, which are expected to greatly facilitate the pathogen detection simply based on the quantitative analysis of fluorescence intensity. To optimize the working concentration of TPE-ARs, their critical aggregation concentrations (CACs) in phosphate buffered saline (PBS) were determined by following the fluorescence changes of TPE-ARs upon aggregation. From the plots of emission intensity of TPE-ARs against their concentrations (Figure 1c), the CAC values of TPE-AMe, TPE-AEt, TPE-APrA, TPE-ABu, TPE-ACH, TPE-ABn, and TPE-AHex in PBS solution can be estimated to be 42.5, 79.2, 47.4, 44.4, 80.2, 76.5, and 65.3×10^{-6} M, respectively, which are in a good agreement with those from the DLS results (Figure S11, Supporting Information). Above CACs, they present diverse aggregate morphologies (Figure S12, Supporting Information). To achieve high detection sensitivity, 20×10^{-6} M of AIEgen PBS solutions with weak fluorescence background were chosen for the following pathogen detection experiments.

2.2. Diverse Fluorescence Response of TPE-ARs with Pathogens

2.2.1. Pathogen Staining and Imaging with TPE-ARs

Seven microorganisms were used as targeted pathogens for demonstration. Among them, *S. aureus*, penicillin-resistant *S. aureus* (abbreviated as *S. aureus*^{R}) and *E. faecalis* are Gram-positive bacteria, *E. coli*, ampicillin-resistant *E. coli* (abbreviated as *E. coli*^{R}) and *P. aeruginosa* are Gram-negative bacteria, and *C. albicans* is a fungus. The addition of these pathogens to seven TPE-ARs solutions gave rise to obvious changes of fluorescence intensity but only little change on the maximum emission wavelength, which greatly facilitates pathogen detection. Taking TPE-APrA for example (**Figure 2**a), after incubating with Gram-positive *S. aureus*^{R}, Gram-negative *E. coli* and fungus *C. albicans*, the fluorescence intensity of TPE-APrA was turned on with different extents, following the order of *C. albicans* > *S. aureus*^{R} > *E. coli*. This reflects the different binding degrees of TPE-APrA to these three pathogens. Meanwhile, the zeta potentials of pathogens did not change distinctly after adding TPE-ARs (Figure 2b), suggesting that these AIEgens inserted into the pathogen membranes or entered the pathogens. This was further confirmed by their confocal microscopy images (Figure 2c). From the confocal images of three AIEgens TPE-APrA, TPE-ACH, and TPE-AHex with seven pathogens, it can be found that these AIEgens not only can efficiently stain the pathogens but also show diverse response signals. Diverse fluorescence responses presented when one strain was incubated with different AIEgens and different strains incubated with the same AIEgen, which is a prerequisite for creating the sensor array to identify pathogens.

2.2.2. Grouping of TPE-ARs Based on Fluorescence Response

To test the ability of seven TPE-ARs to identify pathogens, we used the microplate reader, an easy-to-perform and high-throughput technique, to record the fluorescence intensities of TPE-ARs at 470 nm with the excitation of 340 nm after adding each pathogen. The fluorescence of TPE-ARs alone in PBS was measured as control. The relative fluorescence intensities of TPE-ARs before and after incubation with pathogens,

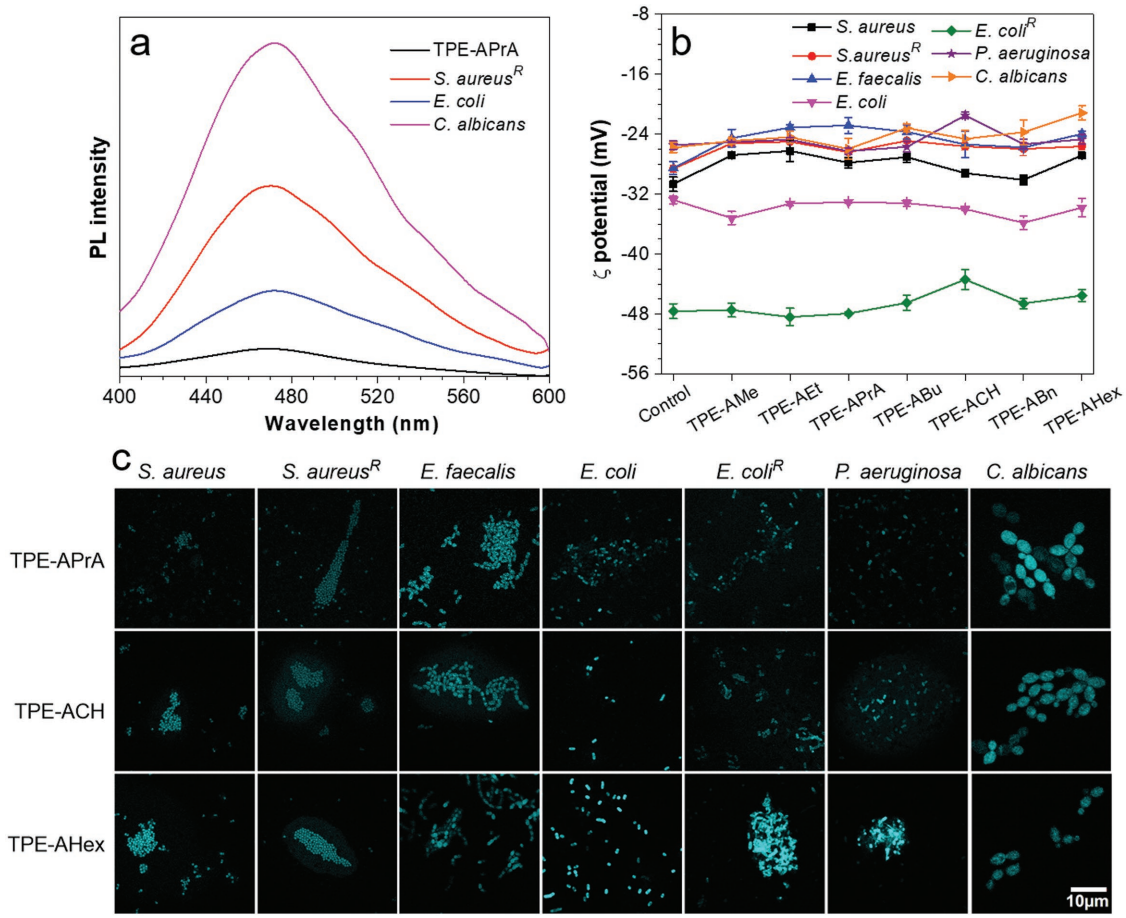

Figure 2. a) Fluorescence spectra of 20×10^{-6} M TPE-APrA in PBS and microbes suspensions. b) Zeta potential results of seven pathogens in the absence and presence of 20×10^{-6} M TPE-ARs. c) CLSM images of seven pathogens after incubation with 20×10^{-6} M AIEgens (TPE-APrA, TPE-ACH, and TPE-AHex) for 15 min. $\lambda_{ex} = 405$ nm and $\lambda_{em} = 430$–500 nm.

$(I - I_0)/I_0$, were used to characterize the fluorescence response for each AIEgen against the seven pathogens. As shown in **Figure 3**, the seven TPE-ARs with *Clog*P values from 3.426 to 6.071 showed diverse fluorescence response signals against the seven pathogens, which should be attributed to the different multivalent interactions between TPE-ARs and pathogens. This explicitly demonstrates the possibility of these AIEgens to identify pathogens.

According to the fluorescence response patterns, we divided the seven TPE-ARs into three groups with the variation of *Clog*P values (Figure 3). The color depth of blue circle was used to describe the relative fluorescence intensity. With the increase of the blue depth, the relative fluorescence intensity increases. For group A, consisting of TPE-AMe, TPE-AEt, and TPE-APrA with $3 < \mathit{Clog}P < 5$, the relative fluorescence intensity of TPE-ARs significantly increases after adding Gram-positive bacteria or fungi, as compared to the Gram-negative bacteria. This was in a good agreement with the observation under the fluorescence microscope as shown in Figure 2c. With *Clog*P value ranging from 5 to 6, group B, including TPE-ABu, TPE-ACH, and TPE-ABn, shows the similar change in the fluorescence intensity between the tested pathogens. Group B was further divided into group B1 (TPE-ACH with larger fluorescence change) and group B2 (TPE-ABu and TPE-ABn with smaller fluorescence change). TPE-AHex with *Clog*$P > 6$ is classified as Group C, which is diametrically opposed to the AIEgens in group A. The relative fluorescence intensity of TPE-ARs in this group shows more increase after adding Gram-negative bacteria than Gram-positive bacteria and fungi. On the basis of these fluorescence responses, we can deduce that with increasing *Clog*P value of TPE-ARs, the affinity of TPE-ARs toward Gram-positive bacteria and fungi was gradually weakened and changed into the higher affinity to Gram-negative bacteria, suggesting that the hydrophobic interaction plays more important role in Gram-negative bacteria compared to Gram-positive bacteria and fungi. Meanwhile, it should be noted that though the fluorescence responses of TPE-ARs to various pathogens are similar in the same group, the extents are still different, implying the variance of the weak interactions between TPE-ARs and pathogens.

2.2.3. Self-Assembly Behavior of TPE-ARs Enriching the Response Difference

It was interesting to observe the emission intensity of TPE-ABu and TPE-AHex was attenuated after incubated with

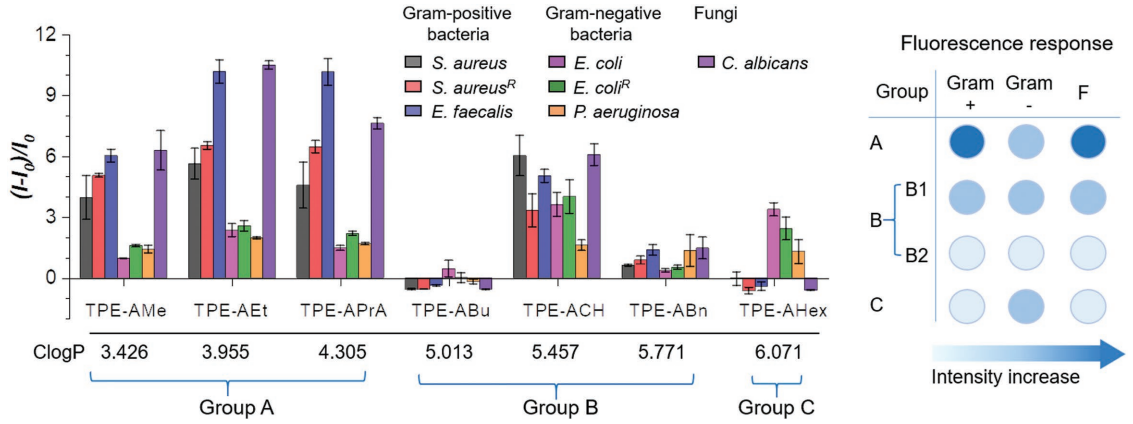

Figure 3. Fluorescence response of seven TPE-ARs after the addition of microbes ($C_{TPE-AR} = 20 \times 10^{-6}$ M) (Left). Each value was the average of six independent measurements, error bar shows the standard deviation of these measurements. λ_{ex}: 340 nm, λ_{em}: 470 nm. I_0 and I are the fluorescence intensity of TPE-ARs in the absence and presence of microbes. The grouping criterion of seven TPE-ARs based on the fluorescence intensity change (Right). The color depth of blue circle stands for the relative fluorescence intensity, that is, with the increase of the blue depth, the change of fluorescence intensity increases.

Gram-positive bacteria and fungi while increased or almost unchanged with Gram-negative bacteria (**Figures** 3 and **4**a). This observation is different from the fluorescence turn-on response of the other TPE-ARs to the pathogens. To understand this interesting phenomenon, we rechecked the fluorescence intensity of seven TPE-ARs below their CAC. It was found that TPE-ABu and TPE-AHex show moderate emission in contrast to the other five AIEgens (Figure 4b). This means that below CAC, TPE-ABu and TPE-AHex tend to form large and loose premicellar aggregates. As demonstrated by the DLS results in Figure 4c, the size distribution of TPE-ABu and TPE-AHex below their CAC (≈1 μm) is much larger than that beyond CAC (≈20 nm for TPE-ABu and ≈100 nm for TPE-AHex). This is very similar to the reported aggregation behavior of oligomeric surfactants, where they first generate large network-like aggregates below the CAC and transform into small micelles with the increase of their concentration.[22] Based on DLS results and transmission electron microscopy (TEM) images, TPE-ABu and TPE-AHex first form large ribbons and sheets below their CAC (Figure 4d,e), respectively. Beyond CAC, their aggregates changed to spherical aggregates of ≈20 nm for TPE-ABu (Figure S12d, Supporting Information) and smaller sheets of about 100 nm for TPE-AHex (Figure S12g, Supporting Information). The formation of these premicellar aggregations could be attributed that TPE-ABu and TPE-AHex bear the longer hydrophobic chains relative to other TPE-ARs, which provide the stronger hydrophobic interaction. Given that the strength of interaction between pathgens and TPE-ARs was weaker than that between TPE-ARs themselves in the premicellar aggregates, the emission intensity of TPE-ARs could be attenuated after incubating with pathogens according to the restriction of intramolecular motions (RIM) mechanism of AIE.[16] Generally, Gram-positive bacteria and fungi have a relative loose and poriferous cell wall,[23] thus the weaker interaction between pathogens and TPE-ARs cannot effectively restrict the intramolecular motion of TPE-ARs, leading to the attenuated fluorescence compared to that of the original premicellar aggregate. In contrast, as for the Gram-negative bacteria, whose cell wall consists of an outer lipid membrane and a thin cross-linked peptidoglycan network,[23b] the strong hydrophobic interaction between the lipid membrane of bacteria and TPE-ARs greatly restricts the rotation of TPE groups, leading to the increase of fluorescence. This diverse self-assembly behavior of TPE-ARs also enriches the interactions of TPE-ARs with pathogens, contributing to the subtle difference in fluorescence response toward different pathogens.

2.3. Pathogen Identification Using Fabricated Sensor Arrays

2.3.1. TPE-ARs Sensor Arrays for Identifying Pathogen

To make a balance between the diverse response and simplicity of the sensor array, we chose one AIEgen from group A, B, and C (Figure 3) to build up a sensor array. Seven TPE-ARs give 17 combinations of sensor arrays, each consisting of three AIEgens, as shown in Table S2 (Supporting Information). It has been verified that the further decrease of AIEgen number ($n < 3$) will reduce the identification accuracy. To test the capability of the built sensor array, the fluorescence response patterns of pathogens produced by the sensor array were analyzed using the linear discriminant analysis (LDA), a powerful statistical method extensively used in pattern recognition.[24] Taking the sensor array of TPE-APrA, TPE-ACH, and TPE-AHex (the combination of AB1C) as an example, the fluorescence pattern of pathogens (**Figure 5**a) could be transformed to 2D canonical score plot by LDA (Figure 5b). The seven pathogens were well-clustered into seven groups and discriminated completely from each other. Interestingly, the distribution of seven pathogens in the 2D canonical score plot obviously associated with their categories, where Gram-negative bacteria were placed at the left, and the Gram-positive bacteria were at the right. The 100% accuracy of discrimination was achieved and proved by "leave-one-out" cross-validation in LDA, demonstrating that our AIEgen sensor array is highly effective for pathogen identification. Significantly, *E. coli*^{R} and *S. aureus*^{R}

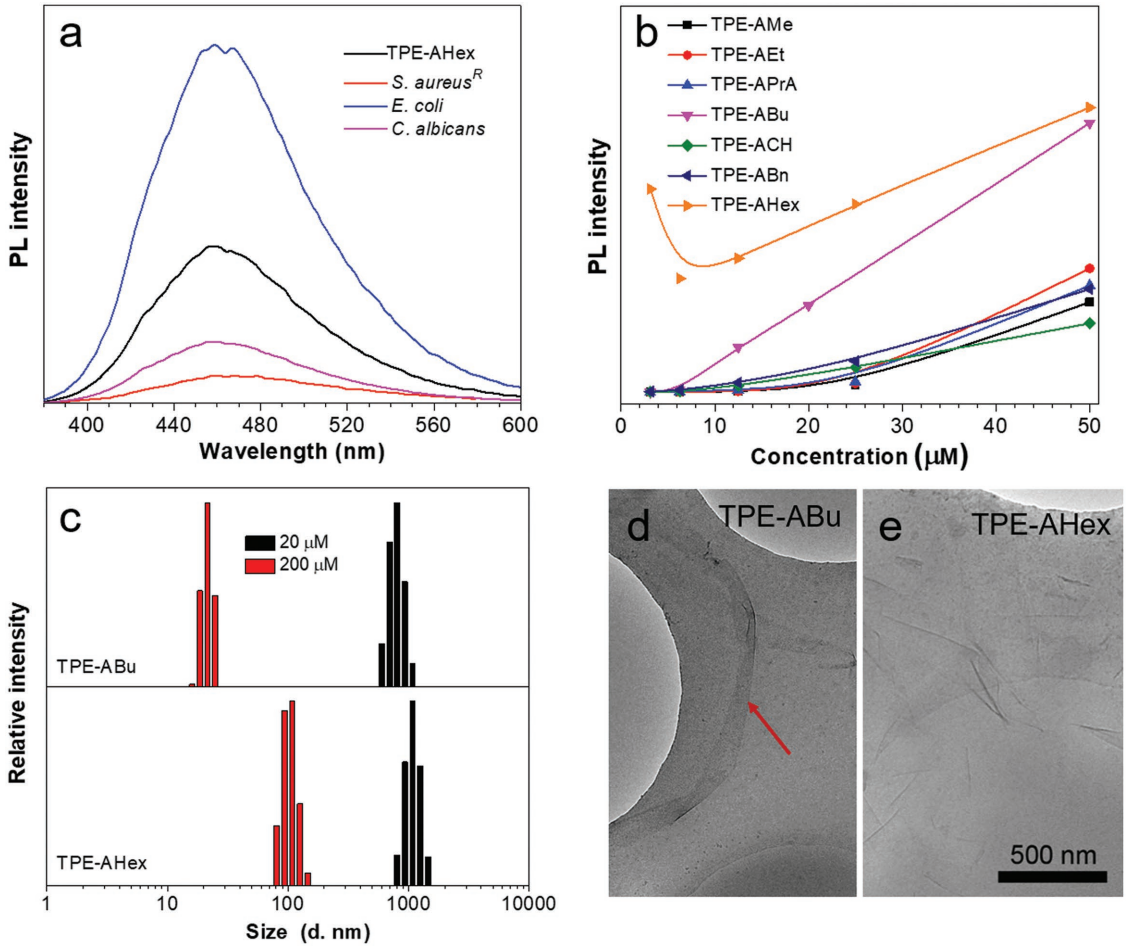

Figure 4. a) Fluorescence spectra of 20×10^{-6} M TPE-AHex in PBS and microbes suspensions. b) Plots of PL intensity of TPE-ARs versus the dye concentration in PBS solution. c) Size distribution of TPE-ABu and TPE-AHex aggregates in PBS solution at the concentration of 20 and 200×10^{-6} M. d,e) Cryo-TEM images of 20×10^{-6} M TPE-ABu and TPE-AHex in PBS solution, respectively.

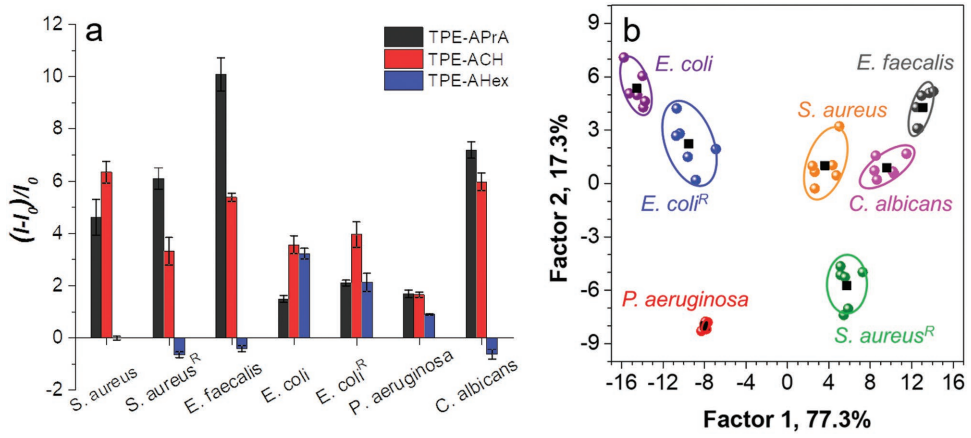

Figure 5. a) Fluorescence response patterns of seven microbes stained by 20×10^{-6} M TPE-APrA, TPE-ACH, and TPE-AHex (combination AB1C) transformed from Figure 3. b) Canonical score plot for the fluorescence response patterns determined by LDA (■ is the centroid of each group and ellipses depict the 95% confidence limits for each pathogen).

can also be easily discerned from normal *E. coli* and *S. aureus* samples by our sensor array, which is very important for effective treatment.

After testing the identification ability of 17 sensor arrays (Figure S13 and Table S2, Supporting Information), 14 out of 17 sensor arrays can achieve 100% classification accuracy for the seven pathogens as well as nearly 100% identification accuracy as proved by cross-validation.

Further to verify the ability of our sensor arrays to predict unknown bacteria, we randomly selected 14 microorganism samples from the seven targeted pathogens. Again, the sensor array consisting of TPE-APrA, TPE-ACH, and TPE-AHex was selected as a representative. Fluorescence response patterns of 14 microorganism samples generated from the sensor array were transformed to the canonical scores by the discriminant functions established from the training samples used in Figure 5. The Mahalanobis distances of a detected sample to the respective centroids of seven groups were calculated in a 3D space (canonical factors 1–3), as shown in Figure S14 (Supporting Information). The shortest Mahalanobis distance value decides the arrangement of pathogen sample. In this way, the 14 unknown samples were completely identified with a detection accuracy of 100%, demonstrating the high reliability of our sensor array (Table S3, Supporting Information).

2.3.2. Fabrication Rule of Sensor Arrays

Based on the above results, we found that TPE-ARs bearing the shorter hydrophobic chain or weaker hydrophobility with $3 < ClogP < 5$ show more selectively binding with Gram-positive bacteria and fungi, whereas those having the longer hydrophobic chain or stronger hydrophobility with $ClogP > 6$ show higher affinity for Gram-negative bacteria. When TPE-ARs present the moderate hydrophobility with $5 < ClogP < 6$, they possess the similar affinity for three kinds of pathogens. The combination of three groups of AIEgens with different hydrophobilities succeeded in generating the competent sensor arrays. In contrast, the introduction of phenyl ring decreases the fluorescence response, leading to the compromised sensitivity and accuracy, as exampled by the sensor arrays TPE-AMe, TPE-ABn, and TPE-AHex; TPE-AEt, TPE-ACH, and TPE-ABn; and TPE-ACH, TPE-ABn, and TPE-AHex (Table S2, Supporting Information). This may be attributed that the additional phenyl ring is a hydrophobic group with large steric hindrance, which could hinder the interaction of TPE core with pathogens. Collectively, the positive charge, hydrophobic substitutions, and the resulted aggregative behavior contribute to the multivalent interactions of TPE-ARs with the pathogens, which greatly augment the diversity in the fluorescence response patterns, contributing to the high detection accuracy.

2.3.3. TPE-ARs Sensor Arrays for Identifying Blends of Pathogens

Practically, the clinical diagnosis often faces the mixed pathogen samples. Thus, the sensor array TPE-APrA, TPE-ACH, and TPE-AHex was also a representative to identify the pathogen mixtures. Eight representative blended samples including four mixtures of two species of microbes and four mixtures of three species of microbes were used as targeted mixed pathogens. Similarly, LDA was used to transform the fluorescence response patterns of pathogen mixtures to 2D canonical score plot, where eight blended pathogens were well-clustered into eight groups with a 100% discrimination accurate (**Figure 6**). Based on the established discriminant function, eight randomly selected blended samples were also completely identified with a detection accuracy of 100% (Table S4, Supporting Information).

3. Conclusion

In summary, we have successfully constructed 14 competent sensor arrays with TPE-based AIEgens for fast and reliable pathogen identification. Each sensor array is composed of three TPE-ARs on the basis of the criterion of balancing the

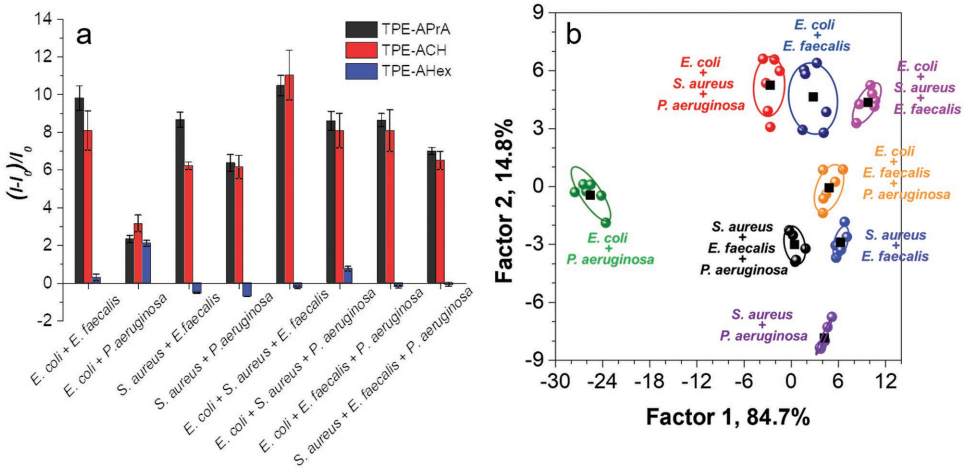

Figure 6. a) Fluorescence response patterns of eight microbe mixtures stained by 20×10^{-6} M TPE-APrA, TPE-ACH, and TPE-AHex (combination AB1C). Each value was the average of six independent measurements, error bar shows the standard deviation of these measurements. λ_{ex}: 340 nm, λ_{em}: 470 nm. I_0 and I are the fluorescence intensity of TPE-ARs in the absence and presence of microbes. b) Canonical score plot for the fluorescence response patterns determined by LDA (■ is the centroid of each group and ellipses depict the 95% confidence limits for each pathogen).

diversity of fluorescence response and simplicity of the sensor array. TPE-ARs bear one cationic ammonium group but different hydrophobic groups with finely controlled hydrophobicity, which were engineered to tune the electrostatic and hydrophobic interactions between AIEgens and pathogens. Meanwhile, TPE-ARs also show diverse aggregate behaviors, further enriching the multivalent interactions of TPE-ARs and pathogens. Thanks to the diverse interactions of TPE-ARs with the pathogens, each sensor array can give a unique fluorescence response pattern for different pathogens. By recognizing the fluorescence pattern of pathogens with assistance of LDA, the seven different pathogens, even normal and drug-resistant bacteria, are identified effectively with nearly 100% accuracy. Also, our sensor arrays are highly suitable for the complicated situations including multiple pathogens. Moreover, the identification procedure is fast (about 0.5 h), very simple without washing steps and high throughput, which exhibits a great potential to offer timely and reliable pathogen information for clinical decisions and monitoring trends of infectious disease. Currently, we are attempting to identify clinical samples using our sensor assays.

4. Experimental Section

Materials and Instrumentations: All the materials and solvents were purchased from the commercial sources (J&K, TCI, and Sigma-Aldrich Company) and used as received. Seven kinds of microorganisms were chosen including three Gram-positive bacteria ((*S. aureus* (ATCC6538), Pen^r*S. aureus* (CGMCC1.879), and *E. faecalis* (JCM5803)), three Gram-negative bacteria (*E. coli* (ATCC25922), Amp^r*E. coli* (TOP10), and *P. aeruginosa* (JCM5962)), and one fungi (*C. albicans* (ATCC10231)), which were purchased from Beijing Bio-Med Technology Development Co., Ltd. and China General Microbiological Culture Collection Center. 1 × PBS (pH 7.4) was used throughout the work. NMR spectra were recorded with a Bruker ARX 400 NMR spectrometer and HRMS were measured in positive mode on a Finnegan MAT TSQ 7000 Mass Spectrometer. UV–vis absorption spectra were recorded on a Milton Ray Spectronic 3000 array spectrophotometer. Fluorescence emission spectra were measured with a Perkin Elmer LS 55 spectromete. The size distribution and zeta potential were measured on Nano ZS (ZEN3600). Laser confocal scanning microscope images were collected on a confocal laser scanning microscopy (FV1200-IX83, Olympus, Japan). Fluorescence intensities of TPE-ARs before and after adding pathogens were recorded on a microplate reader (Varioskan Flash) using black 96-well plates. The morphology of TPE-ARs aggregates was observed by TEM (JEM 2010) and scanning electron microscopy (SEM, S-4300).

*Synthesis of TPE-ARs: Synthesis of 4-(1,2,2-Triphenylvinyl)phenol (**1**)*: Benzophenone (1.82 g, 10 mmol), 4-hydrobenzophenone (1.98 g, 10 mol), and zinc dust (2.60 g, 40 mmol) were placed into a two-necked round-bottom flask. The flask was evacuated under vacuum and refilled with nitrogen three times. Under a nitrogen atmosphere, 70 mL dried tetrahydrofuran (THF) was added, and then 2.2 mL $TiCl_4$ (20 mmol) was slowly added under stirring in dry-ice acetone bath. The reaction mixture was heated to reflux overnight under N_2 protection. After cooling to room temperature, 50 mL dilute hydrochloric acid (1 M) was added to the mixture, and then the mixture was extracted with dichloromethane (DCM). The combined organic phase was dried over anhydrous sodium sulfate and filtered. After the solvent evaporated, the crude product was purified by silica gel column chromatography using *n*-hexane/ethyl acetate (40: 1) as eluent. The white powder was obtained with the yield of 52%. ^{1}H NMR (400 MHz, $CDCl_3$, δ): 7.16–7.09 (m, 8H), 7.07–7.01 (m, 9H), 6.91 (d, J = 8.0, 1H), 6.58 (d, J = 8.0, 1H), 4.78 (s, 1H).

*Synthesis of (2-(4-(2-(2-Bromoethoxy)ethoxy)phenyl)ethene-1,1,2-triyl)-tribenzene (**2**)*: Hydroxylated TPE (**1**) (1.74 g, 5 mmol), dibromoethyl ether (1.39 g, 6 mmol), and K_2CO_3 (1.38 g, 10 mmol) were added in a two-necked round-bottom flask. 30 mL acetone was added under N_2 protection. The reaction mixture was heated to reflux overnight. After solvent evaporation, the crude product was purified by silica gel column chromatography using *n*-hexane/DCM (20: 1) as eluent to give a colorless oil with 65% yield. ^{1}H NMR (400 MHz, $CDCl_3$, δ): 7.13–7.06 (m, 9H), 7.02 (dtd, J = 9.5, 4.6, 2.1 Hz, 6H), 6.95–6.90 (m, 2H), 6.67–6.62 (m, 2H), 4.06 (dd, J = 5.6, 3.8 Hz, 2H), 3.86–3.81 (m, 4H), 3.49–3.46 (m, 2H).

Synthesis of TPE-AR (3): The mixture of (2-(4-(2-(2-bromoethoxy)-ethoxy)phenyl)ethene-1,1,2-triyl)tribenzene (**2**) (2 mmol) and the corresponsing amine (10 mmol) was stirred and heated to reflux in ethanol (20 mL) for 24 h. The solvent was removed under vacuum, and the crude product was repeatedly dissolved by a little methanol, and then excess THF was added to precipitate a white powder, which was dried to obtain the desired compound. The corresponding characterization is as follows:

N,*N*,*N*-Trimethyl-2-(2-(4-(1,2,2-triphenylvinyl)phenoxy)ethoxy)ethan-1-aminium bromide (TPE-AMe): Yield: 82%. ^{1}H NMR (400 MHz, DMSO-d_6, δ): 7.12 (m, 9H), 6.96 (m, 6H), 6.86 (d, J = 8.8 Hz, 2H), 6.70 (d, J = 8.8 Hz, 2H), 4.06–4.00 (m, 2H), 3.88 (m, 2H), 3.78–3.73 (m, 2H), 3.57 – 3.52 (m, 2H), 3.09 (s, 9H). ^{13}C NMR (100 MHz, DMSO-d_6, δ): 156.96, 143.61, 143.53, 143.49, 140.25, 139.91, 135.69, 132.07, 130.79, 130.76, 128.03, 127.93, 126.65, 126.57, 113.84, 68.81, 66.71, 64.54, 64.24, 60.25, 53.29. MALDI-TOF HRMS: calcd. for $C_{33}H_{36}NO_2^+$ [M-Br]$^+$: 478.2741, found: 478.2782.

N-Ethyl-*N*,*N*-dimethyl-2-(2-(4-(1,2,2-triphenylvinyl)phenoxy)ethoxy)-ethan-1-aminium bromide (TPE-AEt): Yield: 84%. ^{1}H NMR (400 MHz, DMSO-d_6, δ): 7.17–7.06 (m, 9H), 6.96 (m, 6H), 6.86 (dd, J = 8.8, 3.3 Hz, 2H), 6.70 (dd, J = 8.8, 3.3 Hz, 2H), 4.07–4.01 (m, 2H), 3.88 (s, 2H), 3.79–3.72 (m, 2H), 3.52 (m, 2H), 3.07 (d, J = 3.2 Hz, 2H), 3.03 (d, J = 3.2 Hz, 6H), 1.22 (m, 3H). ^{13}C NMR (100 MHz, DMSO-d_6, δ): 156.86, 143.49, 143.41143.37, 140.12, 139.74, 135.52, 131.94, 130.67, 130.64, 127.88, 127.78, 126.49, 126.42, 126.38, 113.71, 68.72, 66.58, 63.93, 63.90, 61.78, 59.69, 50.14, 7.98, 7.95. MALDI-TOF HRMS: calcd. for $C_{34}H_{38}NO_2^+$ [M-Br]$^+$: 492.2897, found: 492.2881.

3-Hydroxy-*N*,*N*-dimethyl-*N*-(2-(2-(4-(1,2,2-triphenylvinyl)phenoxy)-ethoxy)ethyl)propan-1-aminium bromide (TPE-APrA). Yield: 86%. ^{1}H NMR (400 MHz, DMSO-d_6, δ): 7.18–7.06 (m, 9H), 7.00–6.92 (m, 6H), 6.86 (d, J = 8.4 Hz, 2H), 6.70 (d, J = 8.4 Hz, 2H), 4.78 (t, J = 5.0 Hz, 1H), 4.06–4.01 (m, 2H), 3.88 (s, 2H), 3.75 (m, 2H), 3.56–3.51 (m, 2H), 3.44 (d, J = 5.0 Hz, 2H), 3.07 (s, 2H), 3.05 (s, 6H), 1.85–1.78 (m, 2H). ^{13}C NMR (100 MHz, DMSO-d_6, δ): 157.36, 144.04, 143.95, 140.73, 140.46, 136.25, 132.53, 131.20, 131.17, 128.54, 128.44, 127.21, 127.13, 127.10, 114.30, 69.39, 67.23, 64.58, 63.13, 62.99, 58.27, 51.65, 25.85, 25.79. MALDI-TOF HRMS: calcd. for $C_{35}H_{40}NO_3^+$ [M-Br]$^+$: 522.3003, found: 522.3058.

N,*N*-Dimethyl-*N*-(2-(2-(4-(1,2,2-triphenylvinyl)phenoxy)ethoxy)ethyl)-butan-1-aminium bromide (TPE-ABu). Yield: 89%. ^{1}H NMR (400 MHz, DMSO-d_6, δ): 7.12 (m, 9H), 7.00–6.92 (m, 6H), 6.86 (d, J = 8.7 Hz, 2H), 6.69 (d, J = 8.7 Hz, 2H), 4.03 (m, 2H), 3.89–3.85 (m, 2H), 3.75 (m, 2H), 3.56–3.51 (m, 2H), 3.28 (d, J = 8.8 Hz, 2H), 3.04 (s, 6H), 1.64 (m, 2H), 1.35–1.25 (m, 2H), 0.84 (s, 3H). ^{13}C NMR (100 MHz, DMSO-d_6, δ): 156.86, 143.48, 143.40, 143.37, 140.11, 139.73, 135.50, 131.92, 130.66, 130.63, 127.86, 127.77, 126.48, 126.39, 126.37, 113.67, 68.73, 66.63, 63.93, 63.87, 62.52, 62.20, 50.78, 50.66, 23.80, 19.22, 19.15. 13.58, 13.49. MALDI-TOF HRMS: calcd. for $C_{36}H_{42}NO_2^+$ [M-Br]$^+$: 520.3210, found: 520.3244.

N,*N*-Dimethyl-*N*-(2-(2-(4-(1,2,2-triphenylvinyl)phenoxy)ethoxy)ethyl)-cyclohexanaminium bromide (TPE-ACH). Yield: 84% yield. ^{1}H NMR (400 MHz, DMSO-d_6, δ): 7.11 (m, 9H), 7.01–6.91 (m, 6H), 6.88–6.83 (m, 2H), 6.72–6.66 (m, 2H), 4.04 (m, 2H), 3.87 (d, J = 6.1 Hz, 2H), 3.80–3.73 (m, 2H), 3.56 (m, 3H), 2.98 (s, 6H), 2.08 (m, 2H), 1.85–1.77 (m, 2H), 1.47–1.18 (m, 6H). ^{13}C NMR (100 MHz, DMSO-d_6, δ): 157.08, 143.72, 143.64, 143.60, 140.37, 140.04, 135.81, 132.18, 130.88, 130.85, 128.13, 128.06, 126.79, 126.69, 113.90, 72.45, 69.07, 66.93, 64.22, 64.16,

61.38, 48.52, 25.68, 25.64, 25.10, 25.04, 24.55. MALDI-TOF HRMS: calcd. for $C_{38}H_{44}NO_2^+$ [M-Br]+: 546.3367, found: 546.3391.

N-Benzyl-*N*,*N*-dimethyl-2-(2-(4-(1,2,2-triphenylvinyl)phenoxy)ethoxy)-ethan-1-aminium bromide (TPE-ABn). Yield: 65%. ^{1}H NMR (400 MHz, methanol-d_4, δ): 7.62–7.52 (m, 9H), 7.07 (m, 7H), 7.00–6.96 (m, 4H), 6.89 (d, J = 8.8 Hz, 2H), 6.67 (d, J = 8.8 Hz, 2H), 4.64 (s, 2H), 4.15 (dd, J = 4.5, 2.3 Hz, 2H), 4.09–4.04 (m, 2H), 3.93–3.86 (m, 2H), 3.65–3.58 (m, 2H), 3.11 (s, 6H). ^{13}C NMR (100 MHz, DMSO-d_6, δ): 156.88, 143.50, 143.42, 143.39, 140.14, 139.77, 135.55, 133.18, 133.15, 132.84, 131.94, 130.69, 130.65, 130.36, 130.33, 128.98, 128.95, 128.91, 128.05, 127.99, 127.89, 127.79, 126.51, 126.42, 113.74, 68.81, 67.46, 67.28, 67.13, 66.62, 64.00, 63.92, 63.14, 62.65, 56.06, 51.78, 49.83, 48.13, 18.57. MALDI-TOF HRMS: calcd. for $C_{39}H_{40}NO_2^+$ [M-Br]$^+$: 554.3054, found: 554.3025.

N,*N*-Dimethyl-*N*-(2-(2-(4-(1,2,2-triphenylvinyl)phenoxy)ethoxy)ethyl)-hexan-1-aminium bromide (TPE-AHex). Yield: 89%. ^{1}H NMR (400 MHz, DMSO-d_6, δ): 7.12 (ddt, J = 13.4, 8.9, 6.5 Hz, 9H), 6.99–6.91 (m, 6H), 6.88–6.83 (m, 2H), 6.72–6.67 (m, 2H), 4.03 (m, 2H), 3.89–3.86 (m, 2H), 3.75 (m, 2H), 3.54 (m, 2H), 3.33–3.27 (m, 2H), 3.05 (s, 6H), 1.63 (m, 2H), 1.27 (m, 4H), 0.94 (t, J = 7.3 Hz, 2H), 0.86 (t, J = 7.3 Hz, 3H). ^{13}C NMR (100 MHz, DMSO-d_6, δ): 156.86, 143.49, 143.42, 143.39, 140.11, 139.74, 135.50, 131.93, 130.67, 130.64, 127.87, 127.79, 127.76, 126.49, 126.40, 113.66, 68.76, 66.64, 64.06, 63.95, 62.18, 50.79, 30.74, 30.66, 25.38, 21.91, 21.84, 21.77, 13.87, 13.82. MALDI-TOF HRMS: calcd. for $C_{38}H_{46}NO_2^+$ [M-Br]$^+$: 548.3523, found: 548.3589.

Preparation of TPE-ARs Solution: The stock solution of 1.0 or 5.0×10^{-3} M TPE-ARs in DMSO was prepared, and diluted to the corresponding concentration with PBS for experiments.

Preparation of Bacteria and Fungi Solution: A single colony of bacteria or fungi on solid agar plate was transferred to 10 mL corresponding liquid culture medium and grown at 37 °C for 6–8 h for bacteria and 30 °C for ≈10 h for fungi (culture medium: LB for *E. coli*, Amp^r *E. coli*, and *P. aeruginosa*, NB for *S. aureus* and Pen^r*S. aureus*, TSB for *E. faecalis*, and YPD for *C. albicans*). Microorganisms were harvested by centrifuging at 7100 rpm for 2 min. The remaining microorganisms were resuspended with PBS, and diluted to an optical density of 1.0 for bacteria and 2.0 for fungi at 600 nm (OD_{600} = 1.0 for bacteria and OD_{600} = 2.0 for fungi).

Experimental Procedure for Pathogen Identification: 40 µL bacteria (OD_{600} = 1.0) or fungi (OD_{600} = 2.0) was transferred to the black 96-well plate, and then 60 µL TPE-AR PBS solution was added with the final volume of 100 µL and the final TPE-AR concentration of 20×10^{-6} M. After shaking for 30 s, the mixtures were incubated at 37 °C for 15 min. Six repeated experiments were performed. All the fluorescence intensities were recorded on a microplate reader with λ_{ex} = 340 nm and λ_{em} = 470 nm. TPE-ARs solution without microbes was also treated under the same conditions as control. The relative fluorescence intensities of TPE-ARs before and after incubation with microbes, that is, $(I - I_0)/I_0$ were calculated by software Microsoft Excel, where I is the fluorescence intensity of TPE-ARs after adding the microbes, and I_0 is the fluorescence intensity of TPE-ARs without microbes. The obtained relative fluorescence intensities $(I - I_0)/I_0$ were introduced in mathematical analysis to receive bacteria identification results by the software IBM SPSS Statistics 22. The whole process only needs about 0.5 h.

Dynamic Light Scattering: The size distribution of TPE-ARs aggregates in organic solvent/water mixtures with water fraction of 96% was measured at 25 °C at a scattering angle of 173° with Nano ZS (ZEN3600) equipped with a thermostated chamber and a 4 mW He–Ne laser (λ = 632.8 nm).

ζ-Potential Measurements: Seven pathogens were incubated by seven TPE-ARs at 37 °C for 15 min, respectively. The microorganisms were harvested by centrifuging at 7100 rpm for 2 min and resuspended in H_2O for zeta potential measurements. The pathogens without TPE-ARs were also treated under the same conditions as control.

Cryo-TEM Measurements: TPE-ARs solutions were placed on freshly carbon-coated holey TEM grids. The excess solutions were removed with filter paper, and then the TEM grids were placed into liquid nitrogen to make the samples embedded in a thin layer of vitreous ice. The frozen samples were observed at 120 kV in low-dose mode by TEM (JEM 2010).

Microorganism Imaging: 500 µL bacteria (OD_{600} = 1.0) or fungi (OD_{600} = 2.0) was transferred to a 1.5 mL centrifuge tube, and harvested by centrifuging (7100 rpm, 2 min). After removing the supernatant, 50 µL of 20×10^{-6} M TPE-ARs PBS solutions were added into the centrifuge tube, and incubated at 37 °C for 15 min. Then 3 µL microorganism solution was added to glass slide and then covered by a coverslip for imaging. The image was collected using CLSM with λ_{ex} = 405 nm and λ_{em} = 430–500 nm.

Supporting Information

Supporting Information is available from the Wiley Online Library or from the author.

Acknowledgements

C.Z. and W.X. contributed equally to this work. The authors thank the staff scientists Dr. Bo Guan, Yang Liu, and Jiling Yue at the Center for Analysis and Testing, ICCAS for their support in cryo-TEM and cryo-SEM measurement. The authors also greatly appreciate the financial support from the National Natural Science Foundation of China (21788102), the Research Grants Council of Hong Kong (16301614, 16308016, 16305015, C6009-17G, C2014-15G, N_HKUST604/14, and A-HKUST605/16), the Innovation and Technology Commission (ITC-CNERC14SC01 and ITS/254117), and the Technology Plan of Shenzhen (JCYJ20160229205601482).

Conflict of Interest

The authors declare no conflict of interest.

Keywords

AIEgens, mathematical analysis, multivalent interaction, pathogen detection, simple and accurate

Received: August 27, 2018
Revised: October 15, 2018
Published online:

[1] a) M. Urdea, L. A. Penny, S. S. Olmsted, M. Y. Giovanni, P. Kaspar, A. Shepherd, P. Wilson, C. A. Dahl, S. Buchsbaum, G. Moeller, D. C. H. Burgess, *Nature* **2006**, *444*, 73; b) X. Didelot, R. Bowden, D. J. Wilson, T. E. Peto, D. W. Crook, *Nat. Rev. Genet.* **2012**, *13*, 601.

[2] "Common Infectious Diseases Worldwide," Infoplease. © 2000–2017 Sandbox Networks, Inc., publishing as Infoplease, https://www.infoplease.com/science-health/health/common-infectious-diseases-worldwide/ (accessed: July 2018).

[3] a) O. Lazcka, F. J. Del Campo, F. X. Munoz, *Biosens. Bioelectron.* **2007**, *22*, 1205; b) A. Duarte, A. Chworos, S. F. Flagan, G. Hanrahan, G. C. Bazan, *J. Am. Chem. Soc.* **2010**, *132*, 12562.

[4] a) B. S. Reisner, G. L. Woods, *J. Clin. Microbiol.* **1999**, *37*, 2024; b) R. P. Peters, M. A. van Agtmael, A. M. Simoons-Smit, S. A. Danner, C. M. Vandenbroucke-Grauls, P. H. Savelkoul, *J. Clin. Microbiol.* **2006**, *44*, 4186.

[5] H. Bai, H. Chen, R. Hu, M. Li, F. Lv, L. Liu, S. Wang, *ACS Appl. Mater. Interfaces* **2016**, *8*, 31550.

[6] A. Borst, A. T. A. Box, A. C. Fluit, *Eur. J. Clin. Microbiol. Infect. Dis.* **2004**, *23*, 289.

[7] a) M. Quesada, M. Giménez, S. Molinos, G. Fernández, M. Sánchez, R. Rivelo, A. Ramírez, G. Banqué, V. Ausina, *Clin. Microbiol. Infect.* **2010**, *16*, 137; b) M.-P. Romero-Gómez, R. Gómez-Gil, J. R. Paño-Pardo, J. Mingorance, *J. Infect.* **2012**, *65*, 513; c) W. Chen, Q. Li, W. Zheng, F. Hu, G. Zhang, Z. Wang, D. Zhang, X. Jiang, *Angew. Chem.* **2014**, *126*, 13954.
[8] M. H. Kollef, *Crit. Care* **2001**, *5*, 189.
[9] a) J. Davies, *Science* **1994**, *264*, 375; b) J. L. Martínez, *Science* **2008**, *321*, 365; c) J. L. Martínez, F. Baquero, D. I. Andersson, *Nat. Rev. Microbiol.* **2007**, *5*, 958; d) M. B. Edmond, S. E. Wallace, D. K. McClish, M. A. Pfaller, R. N. Jones, R. P. Wenzel, *Clin. Infect. Dis.* **1999**, *29*, 239.
[10] F. Walsh, http://www.bbc.com/news/health-30416844 (accessed: December 2014).
[11] A. B. Chinen, C. M. Guan, J. R. Ferrer, S. N. Barnaby, T. J. Merkel, C. A. Mirkin, *Chem. Rev.* **2015**, *115*, 10530.
[12] a) C. Zhu, L. Liu, Q. Yang, F. Lv, S. Wang, *Chem. Rev.* **2012**, *112*, 4687; b) R. L. Phillips, O. R. Miranda, C. C. You, V. M. Rotello, U. H. Bunz, *Angew. Chem., Int. Ed.* **2008**, *47*, 2590; c) H. Yuan, Z. Liu, L. Liu, F. Lv, Y. Wang, S. Wang, *Adv. Mater.* **2014**, *26*, 4333; d) S. Xu, Q. Wang, Q. Zhang, L. Zhang, L. Zuo, J.-D. Jiang, H.-Y. Hu, *Chem. Commun.* **2017**, *53*, 11177; e) H. Pei, J. Li, M. Lv, J. Wang, J. Gao, J. Lu, Y. Li, Q. Huang, J. Hu, C. Fan, *J. Am. Chem. Soc.* **2012**, *134*, 13843.
[13] J. B. Birks, *Photophysics of Aromatic Molecules*, Wiley, New York **1970**.
[14] D. Ding, K. Li, B. Liu, B. Z. Tang, *Acc. Chem. Res.* **2013**, *46*, 2441.
[15] a) H. Jiang, P. Taranekar, J. R. Reynolds, K. S. Schanze, *Angew. Chem., Int. Ed.* **2009**, *48*, 4300; b) N. Cheeveewattanagul, E. Morales-Narváez, A. R. H. Hassan, J. F. Bergua, W. Surareungchai, M. Somasundrum, A. Merkoçi, *Adv. Funct. Mater.* **2017**, *27*, 1702741.
[16] J. Mei, N. L. C. Leung, R. T. K. Kwok, J. W. Y. Lam, B. Z. Tang, *Chem. Rev.* **2015**, *115*, 11718.
[17] a) Y. Yuan, S. Xu, X. Cheng, X. Cai, B. Liu, *Angew. Chem., Int. Ed.* **2016**, *55*, 6457; b) G. Feng, Y. Yuan, H. Fang, R. Zhang, B. Xing, G. Zhang, D. Zhang, B. Liu, *Chem. Commun.* **2015**, *51*, 12490.
[18] J. Heo, S. Z. Hua, *Sensors* **2009**, *9*, 4483.
[19] a) J. Liang, B. Z. Tang, B. Liu, *Chem. Soc. Rev.* **2015**, *44*, 2798; b) R. T. K. Kwok, C. W. T. Leung, J. W. Y. Lam, B. Z. Tang, *Chem. Soc. Rev.* **2015**, *44*, 4228.
[20] G. Liu, S. Tian, C. Li, G. Xing, L. Zhou, *ACS Appl. Mater. Interfaces* **2017**, *9*, 28331.
[21] S. M. Yoo, S. Y. Lee, *Trends Biotechnol.* **2016**, *34*, 7.
[22] a) Y. Hou, M. Cao, M. Deng, Y. Wang, *Langmuir* **2008**, *24*, 10572; b) Y. Fan, Y. Hou, J. Xiang, D. Yu, C. Wu, M. Tian, Y. Han, Y. Wang, *Langmuir* **2011**, *27*, 10570.
[23] a) W. L. Chaffin, J. L. López-Ribot, M. Casanova, D. Gozalbo, J. P. Martínez, *Microbiol. Mol. Biol. Rev.* **1998**, *62*, 130; b) Y. Wang, T. S. Corbitt, S. D. Jett, Y. Tang, K. S. Schanze, E. Y. Chi, D. G. Whitten, *Langmuir* **2012**, *28*, 65.
[24] a) P. Anzenbacher Jr., P. Lubal, P. Buček, M. A. Palacios, M. E. Kozelkova, *Chem. Soc. Rev.* **2010**, *39*, 3954; b) J. R. Askim, M. Mahmoudi, K. S. Suslick, *Chem. Soc. Rev.* **2013**, *42*, 8649.